Brief Report

Not peer-reviewed version

Coherence Thermodynamic Model of Sag A

Jordan Barton *

Posted Date: 27 January 2026

doi: 10.20944/preprints202601.2105.v1

Keywords: black hole thermodynamics; coherence thermodynamics; relativisic jet

Brief Report

Coherence Thermodynamic Model of Sag A

Jordan Barton

Interdependent Researcher; jbiophysics@gmail.com

Abstract

Observations of Sagittarius A* reveal hot spots that orbit and reconstructions feature a trilateral structure. We present a Coherence Thermodynamics model that reproduces these features through interaction with an ellipsoidal field geometry. The previous Cartesian oscillatory field was replaced with an angular form incorporating trilateral symmetry and a radial phase twist representing the black hole's motion through a universal coherence field. This modification yields three dominant observable hot spots with three hidden counterparts, consistent with viewing-angle projection effects. The model was extended to three dimensions and parametrized using physical constants from Sagittarius A* including Schwarzschild radius, corona temperature, and observed orbital period. Results demonstrate that decoherence strength, semantic temperature, certainty ratio, and contradiction-processing intensity form structured patterns in the equatorial and vertical planes. The model suggests black holes function as Mode 2 coherence processors within a trilateral field framework. This work provides a thermodynamic interpretation of relativistic hot spot dynamics consistent with Astrophysical observations.

Keywords: black hole thermodynamics; coherence thermodynamics; relativisic jet

---

1. Introduction

Coherence Thermodynamics provides laws for analyzing contradiction-processing fields in physical systems [1]. Previous work demonstrated that a Cartesian oscillatory field of the form $\sin(2X)\cos(2Y)$ produces four hot spots distributed with bilateral symmetry in a 2-D model of a Coherence and Information processor. However, Event Horizon Telescope observations of Sagittarius A* reveal a more complex structure: hot spots that appear and disappear with the best reconstructions indicating three dominant features during certain orbital phases [2].

This observational constraint motivated a fundamental revision of the field geometry. We replaced the Cartesian oscillation with an angular field based on $\cos(3\theta)$, introducing natural trilateral symmetry. This choice aligns with the ellipsoidal structure hypothesis of the universe and the trilateral symmetry expected from Mode 2 coherence processors—systems that resolve contradictions through distributed processing centers.

Second, we incorporated physical parameters from Sagittarius A* observations, including black hole mass, Schwarzschild radius, corona temperature, accretion disk temperature, and the observed 30-minute orbital period of hot spot flares. A radial phase twist term ωR was added to model the black hole's motion relative to the universal coherence field it interacts with.

Third, we extended the model from two to three spatial dimensions, examining both horizontal (equatorial) and vertical (meridional) slices through the field structure. Two phase twist values were explored: a small twist ($\omega = 0.005$) and a larger twist ($\omega = 0.5$), representing different interaction regimes.

The resulting framework predicts hot spot velocities of approximately $0.3c$ at characteristic radii of $6r_s$, six-fold symmetric field structures with three observable and three hidden processing centers, and structured patterns in decoherence strength, semantic temperature, certainty ratio, and contradiction intensity that emerge naturally from the field geometry.

2. Materials and Methods

2.1. Use of Large Language Models

Large language models (LLMs) were used as technical assistants during this project for: (1) generating and refining Python code to implement Coherence Thermodynamics simulations; and (2) assisting with LaTeX formatting and manuscript structure. All scientific concepts, model design choices, parameter selections, and interpretations were made by the author. All LLM-generated content was reviewed, verified, and edited by the author prior to inclusion.

2.2. Field Geometry Modification

The previous contradiction field:

$$\sigma_{\text{old}} = \exp\left(-(X^2 + Y^2)\right) \sin(2X) \cos(2Y) \tag{1}$$

was replaced with an angular form incorporating trilateral symmetry and radial phase twist:

$$\sigma(x, y, z) = \exp\left(-\frac{X^2 + Y^2 + Z^2}{\sigma^2_{\text{width}}}\right) \cos(3\theta + \omega R) \tag{2}$$

where

$$\theta = \arctan 2(Y, X), \quad R = \sqrt{X^2 + Y^2 + Z^2} \tag{3}$$

This modification implements:

- Cartesian oscillation $\rightarrow$ angular oscillation
- Bilateral symmetry $\rightarrow$ trilateral symmetry
- 4 hot spots $\rightarrow$ 3 dominant + 3 hidden spots
- Static field $\rightarrow$ phase-twisted field (motion through universal field)

The phase structure is defined by:

- **Trilateral angular symmetry:** 3θ creates three-fold rotational symmetry
- **Radial phase twist:** ωR introduces radial variation representing motion

Figures 1 1 and 2 1 use no phase twist $\omega R = 0$ in the Ellipsoidal field model.

Figures 3 3 and 4 4 use a phase twist $\omega R = 0.5$ in the Phase Twist model of Sag A.

Figures 5 5 and 6 6 feature horizontal and vertical images with small phase twist value of $\omega R = 0.005$ in the Phase Twist model of Sag A

Figures 7 7 and 8 8 feature horizontal and vertical images with medium phase twist value of $\omega R = 0.5$ in the Phase Twist model of Sag A.

2.3. General Behavior Across Ellipsoidal Geometries

All ellipsoidal geometries tested were very flat oblate, slightly oblate, and triaxial—produced nearly identical thermodynamic structures in experiments we tried. This indicates that dominant features arise regardless of the ellipsoidal model of the field we chose, which led use to use just one ellipsoidal model in this paper.

2.4. Physical Parameters from Sagittarius A*

All simulations used observationally-derived parameters:

Table 1. Sagittarius A* Physical Parameters.

Parameter	Value	Source
Black hole mass	$4.15 \times 10^6\ M_\odot$	[3]
Schwarzschild radius	1.23×10^{10} m	Calculated
ISCO radius	$4.5\, r_s$	Kerr metric, $a \sim 0.9$
Corona temperature (X-ray)	10^{10} K	[4]
Disk temperature (NIR)	10^7 K	[5]
Hot spot orbital period	30 min	[2]
Hot spot velocity	0.3–0.4c	[2]

2.5. Thermodynamic Quantities

The following quantities were computed throughout the 3D spatial domain:

Decoherence strength:

$$\Gamma = \frac{|\nabla\sigma|^2}{1 + |\nabla\sigma|^2} \tag{4}$$

Semantic temperature:

$$T^\star = T_{\text{disk}} + (T_{\text{corona}} - T_{\text{disk}})\frac{|\nabla\sigma|}{|\nabla\sigma|_{\max}} \tag{5}$$

Semantic heat flux (velocity field):

$$\mathbf{j}_{\text{sem}} = -k_{\text{sem}} \nabla T^\star \tag{6}$$

where $k_{\text{sem}} = 10^{10}\ \text{m}^2/(\text{s}\cdot\text{K})$ was adjusted to match observed hot spot velocities of $\sim 0.3c$.

Certainty ratio:

$$R = \frac{\Delta C_T \cdot \Delta I}{\hbar} = \frac{\xi}{T^\star |\sigma|} \cdot \alpha_I \left(\frac{|\nabla\sigma|}{|\nabla\sigma|_{\max}}\right)^2 \tau_{\text{ref}} \tag{7}$$

where $\tau_{\text{ref}} = 1800$ s (observed orbital period) and $\alpha_I = 10^{-17}\ \text{J}^2\cdot\text{s}$.

Contradiction intensity:

$$S_{\text{sem}} = k_B \ln\left(\frac{1}{C_S}\right), \quad C_S = \exp\left[-\left(\frac{|\nabla\sigma|}{G_0}\right)^{1.5}\right] \tag{8}$$

where $G_0 = \sqrt{\langle|\nabla\sigma|^2\rangle}$.

Free energy:

$$F_{\text{sem}} = E_{\text{sem}} - T^\star S_{\text{sem}} \tag{9}$$

2.6. Three-Dimensional Extension

The model was extended to three dimensions by computing:

$$\nabla\sigma = \left(\frac{\partial\sigma}{\partial x}, \frac{\partial\sigma}{\partial y}, \frac{\partial\sigma}{\partial z}\right) \tag{10}$$

Horizontal slices (equatorial plane, $z = 0$) and vertical slices (meridional plane, $y = 0$) were extracted to visualize the field structure. All thermodynamic quantities were computed identically to the 2D model.

2.7. Computational Implementation

Simulations were performed on grids of 200×200 (2D) and $80 \times 80 \times 80$ (3D) points spanning $\pm 15 r_s$. Gradients were computed using second-order finite differences. All code was written in Python using NumPy and Matplotlib. Interactive notebooks are available at:

doi:10.20944/preprints202601.2105.v1

- Ellipsoidal Field Model: https://colab.research.google.com/drive/1ofor8uopLsPr-Xs7kC2nTKYF1rKbLdub
- Sag A* Model with Phase Twist: https://colab.research.google.com/drive/1Pm4FvbJgS-PS_fufh2szv_ZM0vpqSYl4
- 3D Slices: https://colab.research.google.com/drive/1Dj8GQmWT36xxC0Sq4iIE-XONJyvJ0ZWD

3. Results

3.1. General Ellipsoidal Field Model

The baseline ellipsoidal field model (without Sag A* parameters) demonstrates the emergence of structured thermodynamic features from trilateral field geometry (Figures 1 and 2). Decoherence strength shows six distinct regions alternating in intensity. Semantic temperature exhibits hot zones along the trilateral axes. The certainty ratio reveals tetrahedrons, squares, lines, and point-like structures, with a vertical feature resembling a solenoid passing through the origin. Contradiction processing intensity concentrates along the boundaries between field regions.

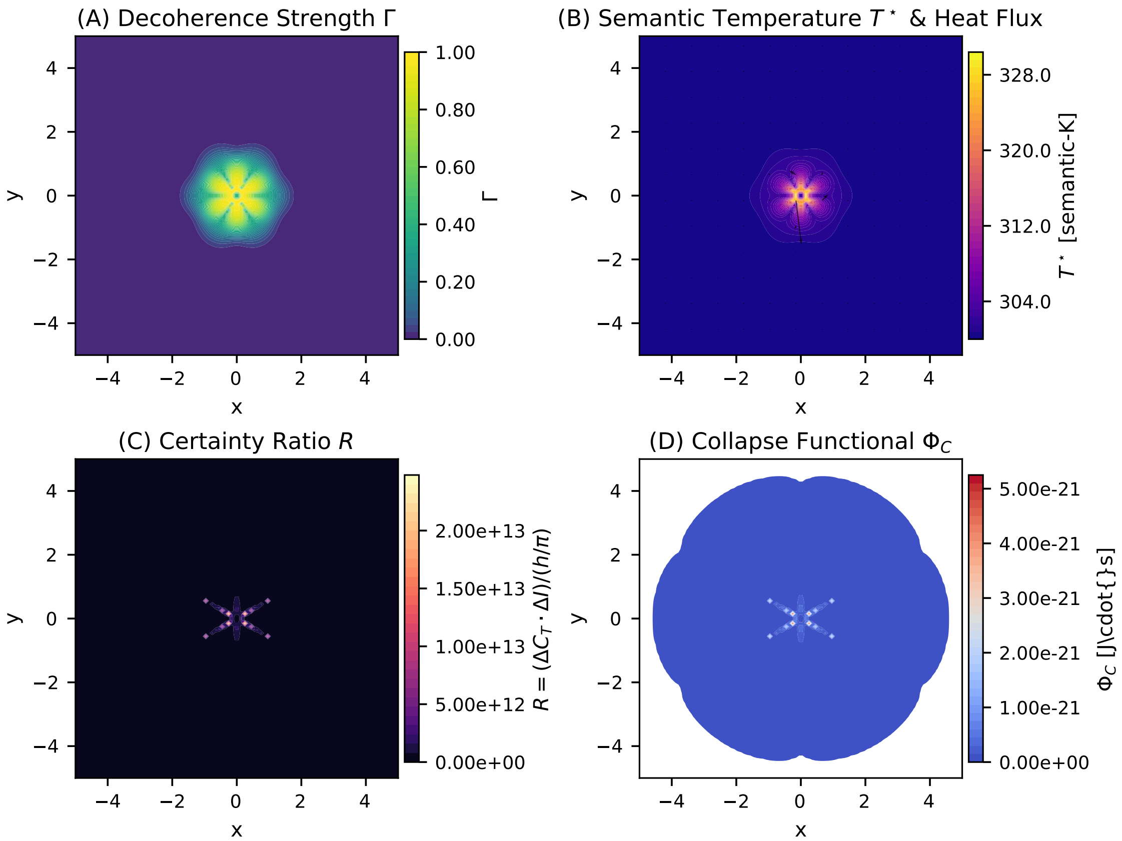

Figure 1. General ellipsoidal field model showing (A) decoherence strength Γ, (B) semantic temperature $T^\star$ with heat flux vectors, (C) certainty ratio R, and (D) collapse functional Φ_C. The trilateral symmetry creates six processing regions in the equatorial plane.

Preprints.org (www.preprints.org) | NOT PEER-REVIEWED | Posted: 27 January 2026 doi:10.20944/preprints202601.2105.v1

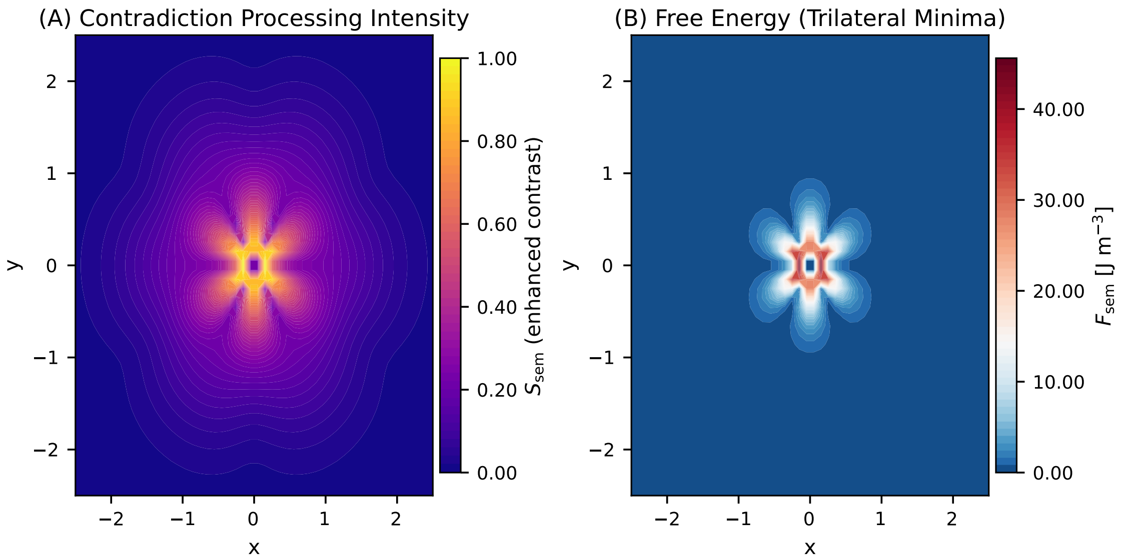

Figure 2. Core dynamics of the ellipsoidal field: (A) contradiction processing intensity and (B) free energy landscape showing trilateral minima structure.

3.2. Sagittarius A Model with Phase Twist*

Incorporating Sag A* physical parameters and a phase twist $\omega = 0.5$ produces features consistent with observations (Figures 3 and 4). The dotted circle in Figure 3, Panel A marks the characteristic hot spot orbital radius.

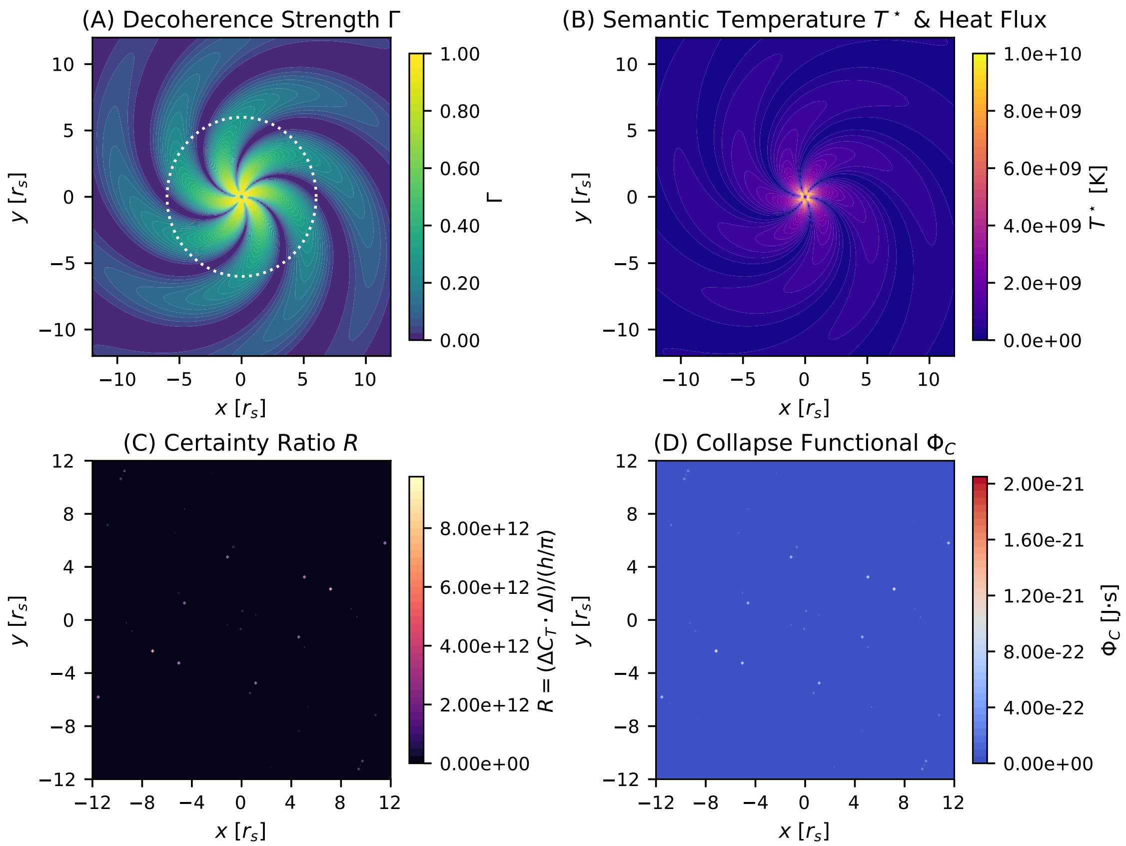

Figure 3. Sag A* model with phase twist showing (A) decoherence strength with hot spot orbital radius marked by dotted circle, (B) semantic temperature distribution, (C) certainty ratio structure, and (D) collapse functional.

Preprints.org (www.preprints.org) | NOT PEER-REVIEWED | Posted: 27 January 2026 doi:10.20944/preprints202601.2105.v1

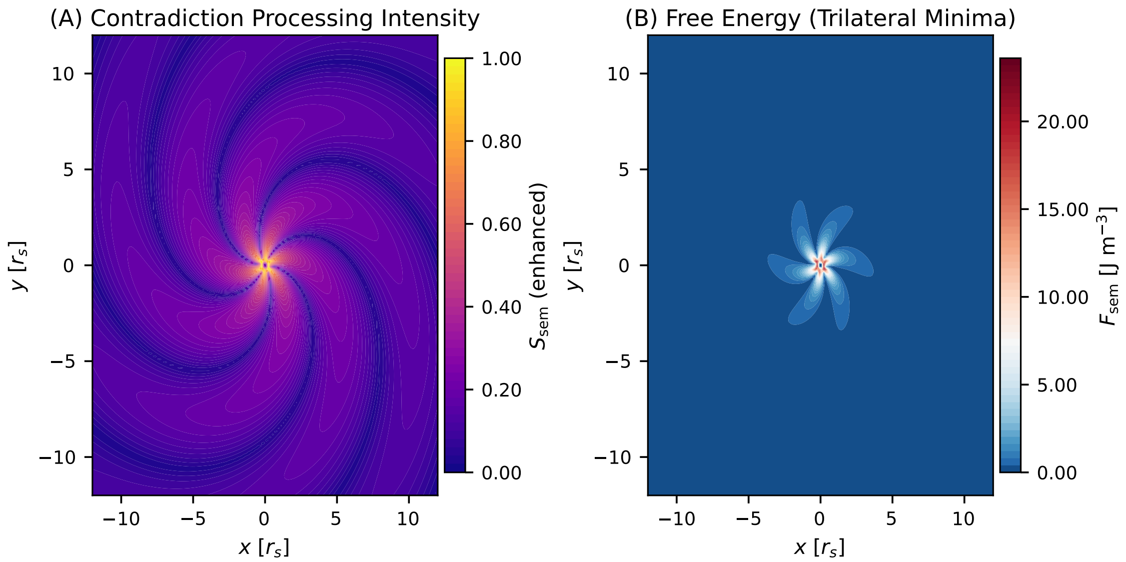

Figure 4. Sag A* core dynamics: (A) contradiction processing intensity showing six-fold structure and (B) free energy minima corresponding to stable processing configurations.

3.3. *Three-Dimensional Field Structure*

The 3D extension reveals how trilateral symmetry manifests in both horizontal and vertical images. Two phase twist regimes were examined:

3.3.1. Small Phase Twist ($\omega = 0.005$)

With minimal radial twist, the field maintains strong six-fold symmetry in horizontal slices (Figures 5 and 6). Vertical slices show symmetric structures about the equatorial plane.

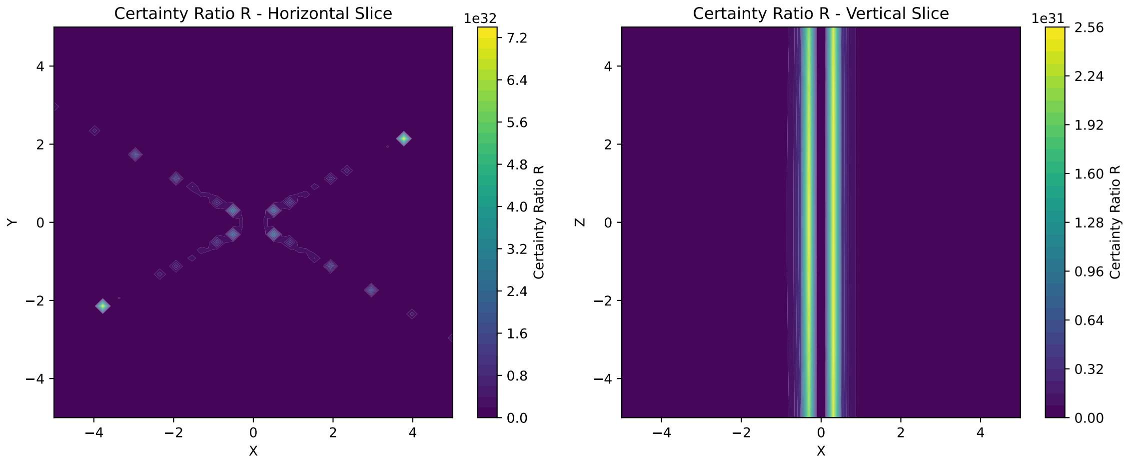

Figure 5. 3D model with small phase twist ($\omega = 0.005$): horizontal and vertical slices of certainty ratio showing six-fold equatorial symmetry and slighlty asymmetric vertical structure.

 doi:10.20944/preprints202601.2105.v1

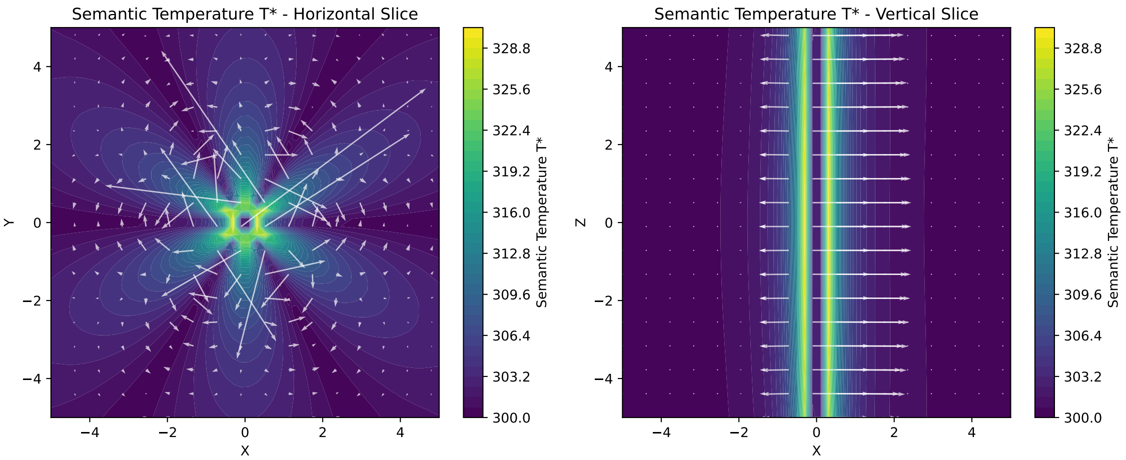

Figure 6. Temperature distribution in 3D with small phase twist: horizontal and vertical slices revealing thermal structure of the trilateral field.

3.3.2. Large Phase Twist ($\omega = 0.5$)

Increased radial twist introduces helical structure while preserving trilateral symmetry (Figures 7 and 8). This configuration models stronger coupling between black hole motion and the background field. Vertical slices show asymmetry consistent with a twisted solenoid-like structure, potentially relevant to jet collimation.

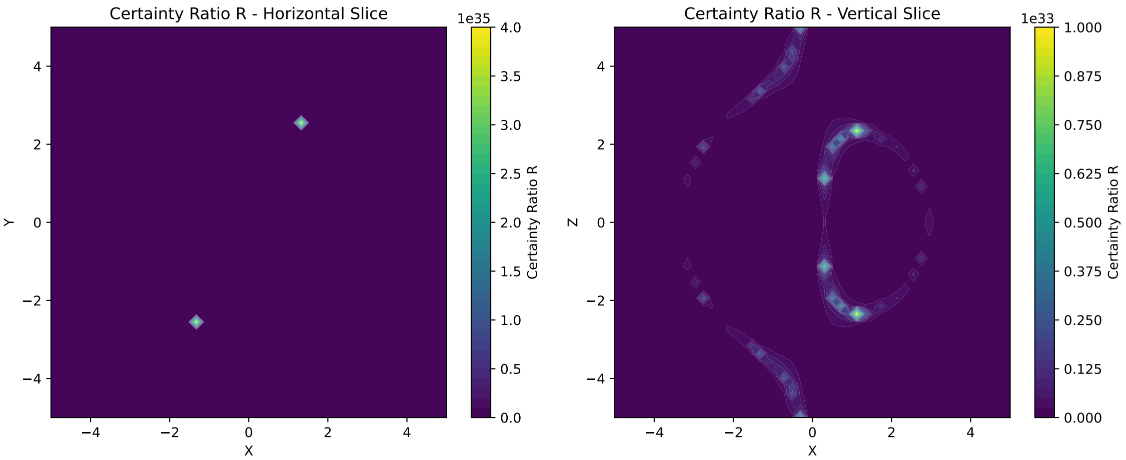

Figure 7. 3D model with large phase twist ($\omega = 0.5$): horizontal slices show reduced symmetry and vertical slices of certainty ratio showing twisted structure and circular feature.

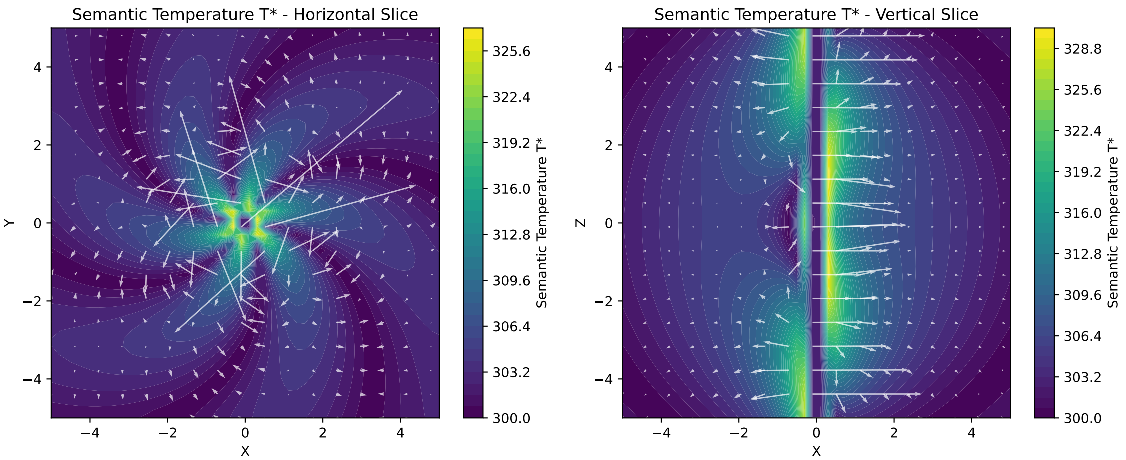

Figure 8. Temperature distribution in 3D with large phase twist: twisted thermal structure potentially relevant to relativistic jet formation and collimation.

doi:10.20944/preprints202601.2105.v1

3.4. Velocity and Temperature Profiles

Analysis of semantic velocities and temperatures at different radii confirms the model's consistency with observational constraints.

Table 2. Semantic Velocity and Temperature vs. Radius.

Radius $[r_s]$	Mean v [m/s]	Max v [m/s]	Max/c	Mean T [K]	Max T [K]
1.00	6.240×10^9	1.073×10^{10}	35.792	2.796×10^9	5.049×10^9
2.22	1.482×10^9	2.545×10^9	8.490	1.295×10^9	2.110×10^9
3.44	7.184×10^8	1.190×10^9	3.970	8.934×10^8	1.429×10^9
4.67	4.445×10^8	7.451×10^8	2.485	6.931×10^8	1.104×10^9
5.89	3.216×10^8	5.285×10^8	1.763	5.797×10^8	9.181×10^8
7.11	2.522×10^8	4.140×10^8	1.381	4.985×10^8	7.840×10^8
8.33	2.046×10^8	3.367×10^8	1.123	4.352×10^8	6.824×10^8
9.56	1.701×10^8	2.809×10^8	0.937	3.799×10^8	5.951×10^8
10.78	1.437×10^8	2.378×10^8	0.793	3.331×10^8	5.197×10^8
12.00	1.210×10^8	2.031×10^8	0.678	2.896×10^8	4.529×10^8

Peak velocity and temperature in this model occur at $r \sim 1{-}r_s$ and descend as radius increases away from the processing core.

4. Discussion

4.1. Hot Spot Velocity and Structure

Event Horizon Telescope observations indicate hot spots orbiting Sagittarius A* at approximately 0.3–0.4c [2]. While precise hot spot counts vary between reconstruction methods, the best analyses suggest three dominant features during certain orbital phases. Our model attempts to reproduces these velocities at characteristic radii of $6r_s$ through the semantic conductivity parameter k_{sem}, which represents the propagation speed of coherence information through the field.

The trilateral field geometry naturally produces six processing centers (Figure 1: which we predict will manifest as three on the near side (observable, Doppler-boosted) and three on the far side (hidden or suppressed by viewing angle). This 3+3=6 structure arises directly from the $\cos(3\theta)$ angular dependence and is consistent with projection effects expected for an observer located ~ 8 kpc from Sagittarius A*.

Owing to the inclined viewing geometry of Sagittarius A*, relativistic beaming enhances near-side emission while suppressing receding and far-side components. Gravitational lensing further redistributes far-side emission into weaker or overlapping structures. As a result, an underlying six-fold emission pattern can appear observationally as three dominant hot spots on the near side.

4.2. Phase Twist and Motion Through the Universal Field

The radial phase twist term ωR models the black hole's motion relative to a universal coherence field, which introduces Helical structure in vertical slices, Asymmetry between approaching and receding field lines and a potential connection to jet collimation mechanisms.

Larger twist values ($\omega = 0.5$) in Figure 8 produce twisted solenoid-like structures in the vertical plane, which may relate to the helical knots observed in M87's relativistic jet. The collimation and stability of such jets could be maintained by the coherence acting on the information-resolving substrate. The largest temperature values in this model occur close to the center of the model, indicating a potential super-phase that exists inside a black hole.

The twisted certainty ratio nodes in vertical slices provide a structural interpretation for features observed in relativistic jets. Observed emission knots exhibit that exhibit helical progression: As shown by Park et al. ([6]), the M87 jet is consistent with a large-scale helical magnetic field that naturally organizes emission into knotty, quasi-helical structures. The parallel-plate-like progression observed in some jets may emerge from stacked, horizontally coherent zones within the magnetized flow, while the apparent helical twist reflects jet plasma following twisted field lines anchored near the black hole. If the surrounding or "universal" field has its own characteristic frequency and phase structure, the resulting jet morphology may alternate between predominantly parallel-plate features, less symmetric patterns, and clearly helical configurations.

We propose that jets in black holes are not solely in one mode for jet formation. We propose the jet will not always be helical or chaotic or resemble parallel plate features at times, but that the jets characteristic patterns are a result of the black hole as a coherence and information processor interacting and checking its answers against the universal field. Our past research [1] has proposed this field, and we believe the observational features of black holes and our model, apparent max velocities in table 2 2 slightly exceeding the speed of light near the core of the model. We believe this model still holds and further work is to be done to make this model more accurate.

4.3. What are the Hot Spots?

Figure 3, panel A 3 shows a slightly decoherence plot emanating from the black hole processors core. We propose that as the black hole processes information in front of it, that it also produces decoherence's as a result in the surrounding environment. As the black hole processor see's information, certain information takes more processing power and carries more entropy than others. This results in ebbs and tides as hot spots appear and disappear in chaotic or even symmetric patterns.

4.4. Future Observational Tests

Predictions from this model that could be tested with future Event Horizon Telescope observations include Six-fold symmetry in time-averaged hot spot distributions, with three hidden hot spots, varying structure in jet emission and that the hot spots are literally the decoherence events that are so large they finally register as hot spots.

5. Conclusions

We have presented a Coherence Thermodynamics model of Sagittarius A* hot spots based on trilateral ellipsoidal field geometry. The replacement of Cartesian oscillation with angular field structure $\cos(3\theta + \omega R)$ produces three dominant observable hot spots with three hidden counterparts. We have shown structured decoherence, temperature, and certainty patterns. Jet structures are potentially related to the black hole's processing dynamics as it moves through and interacts with the universe and its coherence field. The model strengthens the notion that black holes function as Mode 2 coherence processors. The phase twist represents motion through this field, and the semantic conductivity parameter connects field gradients to observable velocities.

This work demonstrates that Coherence Thermodynamics provides a consistent set of laws for interpreting relativistic hot spot dynamics around supermassive black holes. Future refinements will expand this model.

Author Contributions: The Author is solely responsible for all generated content.

Funding: Not Currently Funded

Data Availability Statement: Our codes our openly available for this paper in Colab: • Ellipsoidal Field Model: https://colab.research.google.com/drive/1ofor8uopLsPr-Xs7kC2nTKYF1rKbLdub • Sag A* Model with Phase Twist: https://colab.research.google.com/drive/1Pm4FvbJgS-PS_fufh2szv_ZM0vpqSYl4 • 3D Slices: https://colab.research.google.com/drive/1Dj8GQmWT36xxC0Sq4iIE-XONJyvJ0ZWD

Acknowledgments: The Author is grateful for his constitutional rights, which enable this individual led research. This research is dedicated to all those who have defended this sacred charter of the United States of America.

Conflicts of Interest: The authors declare no conflicts of interest.

doi:10.20944/preprints202601.2105.v1

Abbreviations

The following abbreviations are used in this manuscript:

CT	Coherence Thermodynamics
EHT	Event Horizon Telescope
ISCO	Innermost Stable Circular Orbit
NIR	Near-Infrared
Sag A*	Sagittarius A*

References

1. Barton, J. From Decoherence to Coherent Intelligence: A Framework for the Emergence of AI Structure through Recursive Reasoning. *Preprints* **2025**, *2025*. https://doi.org/10.20944/preprints202504.1917.v6.
2. Event Horizon Telescope Collaboration. First Sagittarius A* Event Horizon Telescope Results. I. The Shadow of the Supermassive Black Hole in the Center of the Milky Way. *Astrophysical Journal Letters* **2022**, *930*, L12.
3. GRAVITY Collaboration. Detection of the gravitational redshift in the orbit of the star S2 near the Galactic centre massive black hole. *Astronomy and Astrophysics* **2018**, *615*, L15.
4. Neilsen, J.; Nowak, M.A.; Gammie, C.F.; Dexter, J.; Markoff, S.; Haggard, D.; Baganoff, F.K.; Barrière, N.M.; Degenaar, N.; et al.. A Chandra/HETGS Census of X-ray Variability from Sagittarius A*. *The Astrophysical Journal* **2013**, *774*, 42. https://doi.org/10.1088/0004-637X/774/1/42.
5. Boyce, H.; Haggard, D.; Witzel, G.; von Fellenberg, S.; Willner, S.P.; Becklin, E.E.; Do, T.; Eckart, A.; Fazio, G.G.; Gurwell, M.A. Multiwavelength Variability of Sagittarius A* in 2019 July. *The Astrophysical Journal* **2022**, *931*, 7. https://doi.org/10.3847/1538-4357/ac6104.
6. Park, J.; Asada, K.; Nakamura, M.; Pu, H.Y.; Algaba, J.C.; Inoue, M.; Honma, M.; et al. Helical Magnetic Field in the Acceleration–Collimation Zone of the M87 Jet. *The Astrophysical Journal Letters* **2026**. in press; see arXiv preprint.